Role of physical processes controlling oxycline and suboxic layer structures in the Black Sea

Temel Oguz
Institute of Marine Sciences, Middle East Technical University, Erdemli, Icel, Turkey

Received 10 July 2001; revised 20 November 2001; accepted 23 January 2002; published 15 May 2002.

[1] A one-dimensional coupled physical-biogeochemical model, together with reanalysis of the available data, are used to provide a new perspective for identification and interpretation of the suboxic layer (SOL) of the Black Sea. While the lower boundary appears to be stable at $\sigma_t \approx 16.15 \pm 0.10$ kg m^{-3}, the upper boundary is found not to be isopycnally uniform as asserted previously. It is found to vary depending on the intensity of vertical diffusive and advective oxygen fluxes across the oxycline. Its position, therefore, does not always correspond to a distinct density surface irrespective of the circulation characteristics. Instead, it changes from $\sigma_t \approx 15.55 \pm 0.1$ in cyclonic to $\sigma_t \approx 15.9 \pm 0.1$ kg m^{-3} in anticyclonic regions, whereas its position in the peripheral Rim Current transition zone occurs at intermediate density values. These findings imply that vertical oxygen variations cannot be expressed in terms of density without taking into account physical characteristics of the water column. The presence of very strong density stratification is found to prevent ventilation of the SOL. Even intense turbulent mixing generated by a large buoyancy loss during an exceptionally cold winter season is unable to generate sufficiently dense water to overturn and temporarily supply oxygen into the suboxic zone. *INDEX TERMS:* 4572 Oceanography: Physical: Upper ocean processes; 4802 Oceanography: Biological and Chemical: Anoxic environments; 4815 Oceanography: Biological and Chemical: Ecosystems, structure and dynamics; 4842 Oceanography: Biological and Chemical: Modeling; 4845 Oceanography: Biological and Chemical: Nutrients and nutrient cycling; *KEYWORDS:* Black Sea, suboxic layer, biogeochemical modeling, physical processes, isopycnal uniformity

1. Introduction

[2] Beginning with the R/V *Knorr* measurements in 1988 [*Friederich et al.*, 1990; *Murray*, 1991; *Codispoti et al.*, 1991], the data collected during the 1990s in different seasons and regions of the Black Sea [*Tugrul et al.*, 1992; *Saydam et al.*, 1993; *Basturk et al.*, 1994, 1997] has consistently shown the presence of a stable oxygen-deficient zone with $O_2 \leq 10$ μM (known as the suboxic layer (SOL)). It has been suggested that the upper and lower boundaries of the SOL correspond to fixed density surfaces of $\sigma_t \approx 15.6$ and $\sigma_t \approx 16.2$ kg m^{-3}, respectively, which are independent of the circulation characteristics of the basin. The idea of isopycnal uniformity of the boundaries of the SOL originated when the 1988 *Knorr* oxygen data were plotted with respect to density. A composite plot of all profiles from different stations (Figure 1b) showed a reasonably uniform oxygen structure involving a uniform slope within the oxycline, followed by concentrations of <10 μM in the SOL. The same approach, applied to 1991 R.V. *Bilim* data (Figure 1c), showed more variability both in the oxycline and suboxic zones. Oxygen concentrations of >10 μM inside the $\sigma_t \approx 15.6$ and $\sigma_t \approx 16.2$ kg m^{-3} density boundaries were interpreted as analytical errors due to atmospheric contamination of water samples rather than due to regional variability. Isopycnal uniformity in the concentration of biogeochemical variabilities implicitly assumes that vertical processes do not play a major role in controlling their distributions. This assumption has never been explicitly verified by providing specific maps of property distributions or by quantitatively simulating the relative magnitudes of vertical versus horizontal physical processes for both cyclonic and anticyclonic circulation regimes. The present work uses the available data and uses a relatively simple one-dimensional (1-D) coupled physical-biogeochemical model to address these issues. More specifically, it (1) explores how the SOL structure is controlled by vertical advection and diffusion and (2) assesses whether the boundaries of the SOL always correspond to distinct density surfaces irrespective of the circulation characteristics. When investigating the role of diffusion, we also attempt to clarify the possible ventilation of the SOL by convective mixing during strong cooling events.

2. Model Formulation

[3] The model essentially follows the one given by *Oguz et al.* [2000] describing the dynamically coupled oxic-suboxic-anoxic system of the Black Sea water column. It consists of 14 state variables (Table 1) involving two groups of phytoplankton (diatoms and phytoflagellates), nonphotosynthetic free-living bacterioplankton, microzooplankton with a size of <200 μm (dominated by heterotrophic flagellates and ciliates), mesozooplankton with a size of 0.2–2 mm (consisting of copepods, cladocerans, and appendicularians), gelatinous carnivorous medusae *Aurelia aurita*, opportunistic species omnivorous dinoflagellate *Noctiluca scintillans*, particulate and dissolved organic nitrogen, ammonium, nitrate, nitrogen gas, dissolved oxygen, and hydrogen sulfide. Schematic presentations of the food web structure, nitrogen, and redox cycling have been provided by *Oguz et al.* [2000, Figures 3a and 3b]. The local temporal variations of all biogeochemical variables are expressed by a set of diffusion-advection-reaction equations of the general form

$$\frac{\partial F}{\partial t} = \frac{\partial}{\partial z}\left[(K_b + \nu_b)\frac{\partial F}{\partial z} - (w - w_b)F\right] + \Re(F), \qquad (1)$$

0886-6236/02/2001GB001465$12.00

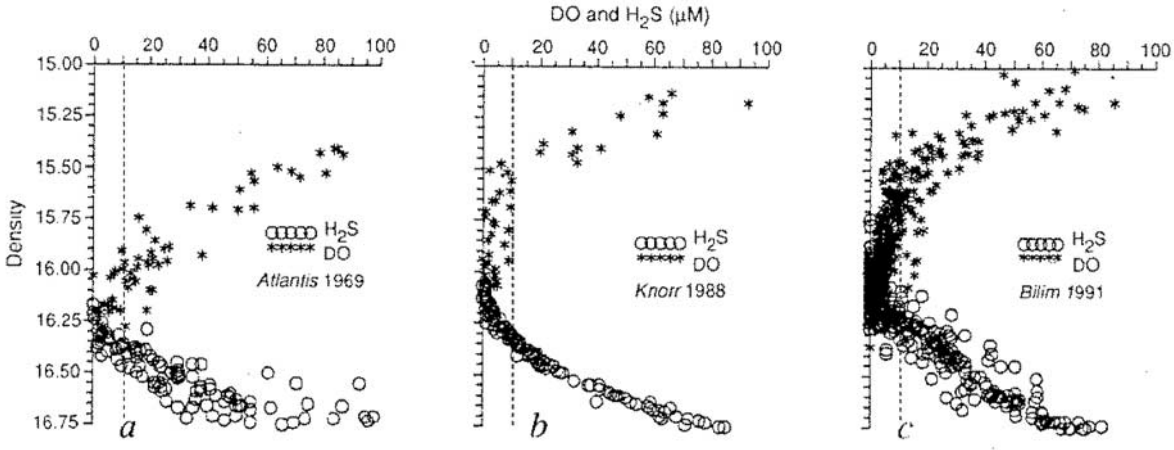

Figure 1. Composite profiles of dissolved oxygen (DO) and hydrogen sulfide relative to density (in σ_t) for (a) *Atlantis* 1969 data (30 stations), (b) *Knorr* 1988 data (5 stations), and (c) *Bilim* 1991 data (46 stations) [after *Tugrul et al.*, 1992].

where F denotes any state variable of the biogeochemical model given in Table 1, t is time, z is the vertical coordinate directed upward from the sea surface, ∂ denotes partial differentiation, K_b is the vertical diffusion coefficient associated with the wind and buoyancy induced turbulence near the surface of the water column, ν_b is its background value (representing mixing associated with internal waves), w is the vertical velocity component of the fluid motion (representing both upwelling and downwelling), w_b (≤ 0) denotes the sinking velocity for diatoms and detritus, and $\Re(F)$ denotes the net balance of sources and sinks for each state variable.

[4] The biogeochemical model is coupled with the physical model through specification of vertical eddy diffusivity and temperature. The physical model, which has been documented previously by *Oguz et al.* [1996, 1999], is based on a 1-D version of the Princeton Ocean Model. The vertical diffusion coefficient, K_b, is computed by the Mellor-Yamada order 2.5 turbulence closure scheme embedded within the physical model. The way in which ν_b is represented based on the available observations is given in section 3.

[5] Because we primarily deal with the biogeochemical structure below the euphotic zone, we only include here equations for nitrogen and redox cycling within the nitracline, suboxic, and suboxic-anoxic interface zones. The source-sink terms for particulate and dissolved organic nitrogen, ammonium, nitrate, and nitrogen gas, as well as for dissolved oxygen and hydrogen sulfide, are expressed by

$$\Re(D_p) = [\mathrm{BIO_p}] - R_1 - R_2, \tag{2a}$$

$$\Re(D_d) = [\mathrm{BIO_d}] + (1-\kappa)R_1 + R_2, \tag{2b}$$

$$\Re(N_a) = [\mathrm{BIO_a}] + \kappa R_1 - R_3 - R_6, \tag{2c}$$

$$\Re(N_n) = [\mathrm{BIO_n}] + R_3 - \alpha_2 R_2 - R_7 + R_8, \tag{2d}$$

$$\Re(N_2) = \alpha_2 R_2 + R_7 + R_6 - R_8, \tag{2e}$$

$$\Re(O_2) = \alpha_0[\mathrm{BIO_o}] - \alpha_1 R_1 - \alpha_3 R_3 - \alpha_4 R_4, \tag{2f}$$

$$\Re(H_s) = -R_4 - R_5, \tag{2g}$$

where R_k refers to the reaction kinetics given in Table 2 and α_k denotes stoichiometric coefficients, whose values, together with other parameters, are given in Table 3. Equations (2a)–(2g) involve seven reaction kinetics taking place in different parts of the water column. Those denoted by R_1, R_3, and R_4 represent, respectively, the oxidation of particulate material, ammonium, and hydrogen sulfide by dissolved oxygen. R_2 represents denitrification, and R_5 and R_6 involve oxidation of HS^- and NH^- by settling particulate manganese (MnO_2) produced by the reaction of dissolved manganese (Mn^{2+}) with nitrate NO_3^- [*Murray et al.*, 1995; *Luther et al.*, 1997; *Murray et al.*, 1999]. In addition to its contribution from the deeper levels of the anoxic pool, Mn^{2+} is produced locally as a by-product of these reactions and is reoxidized by nitrate. More details on the formulation of redox cycling are given by *Oguz et al.* [2001a]. Following the euphotic zone food web model described by *Oguz et al.* [2001b], [BIO_p] includes the contributions from the unassimilated parts of grazing functions, mortality, and detritus consumptions by various zooplankton groups. [BIO_d] describes the exudation and consumption of dissolved organic matter by bacteria. [BIO_a] and [BIO_n] include ammonium and nitrate uptakes during the phytoplankton production. [BIO_a] also includes contributions from excretion. [BIO_o] involves the oxygen production during photosynthesis. The reactions taking place within the oxygen-depleted part of the water column involve a loss of nitrogen from the system in the form of fixed-nitrogen gas (N_2). In 1-D models

Table 1. State Variables of Biogeochemical Model

Variable	Definition
P_d	diatom
P_f	phytoflagellate
B	bacterioplankton
Z_s	microzooplankton
Z_m	mesozooplankton
Z_n	dinoflagellate *Noctiluca scintillans*
Z_a	gelatinous carnivore *Aurelia aurita*
D_p	particulate organic nitrogen
D_o	dissolved organic nitrogen
N_a	ammonium
N_n	nitrate
N_2	nitrogen gas
O_2	dissolved oxygen
H_s	hydrogen sulfide

Table 2. Reaction Kinetics

Reactions	Definition
$R_1 = \epsilon\left[\frac{O_2}{O_2+R_O}\right]D_p$	aerobic remineralization
$R_2 = \epsilon\left[\frac{K_O}{K_O+O_2}\right]D_p$	unaerobic remineralization
$R_3 = k_3\left[\frac{O_2}{O_2+R_O}\right][N_a]$	nitrification
$R_4 = k_4\ [O_2]\ [H_s]$	oxidation of hydrogen sulfide by dissolved oxygen
$R_5 = k_5\ [MnO_2]\ [H_s]$	oxidation of hydrogen sulfide by particulate manganese
$R_6 = k_6[MnO_2]\ [N_a]$	oxidation of ammonium by particulate manganese
$R_7 = k_7\ [N_n]\ [Mn^{2+}]$	oxidation of dissolved manganese by nitrate
$R_8 = k_8\ [N_2]$	conversion of nitrogen gas into nitrate

with long-term time integration, it is necessary to conserve the amount of total nitrogen in the water column. Therefore these losses must be compensated for somehow. In work by *Oguz et al.* [2000, 2001b] the approach we used was to add an equivalent rate of nitrate concentration to the nitrate maximum zone at each time step. In the present model we follow a slightly different method. By introducing N_2 as an independent state variable in equation (2e), we retain these losses within the water column by converting nitrogen gas back to the nitrate while it diffuses toward upper levels. This process was incorporated into equations (2d) and (2e) by a simple first-order reaction R_8. Even though validity of this reaction in the SOL may be questionable from the biogeochemical point of view, it provides a practical mathematical closure of the model equations.

[6] The boundary conditions at the surface $z = 0$ and the bottom $z = h_b = 150$ m imply the absence of the sum of advective and diffusive fluxes for each state variable. For the diatom and detritus equations, we also specify the absence of export flux of particulate matter from the bottom boundary, implying subsequently complete remineralization within the water column; see *Oguz et al.* [1996, 1999] for a more detailed justification. In the oxygen equation the air-sea exchange of oxygen is expressed by

$$\left[(K_b + \nu_b)\frac{\partial O_2}{\partial z}\right]_{z=0} = V_p\left[O_2^{sat} - O_2(z=0)\right], \qquad (3)$$

where V_p is the piston velocity and O_2^{sat} represents the oxygen saturation concentration computed using the surface temperature and salinity values of the physical model at each time step. The physical model is forced by daily climatological wind stress, net surface heat flux, and surface salinity. It prescribes no-stress, no-heat, and no-salt flux conditions at the bottom boundary, where we also specify H_s and N_a concentrations of 25 and 10 μM, respectively.

[7] The model water column is discretized by introducing 50 vertical levels, providing a grid spacing of ~3.0 m. A time step of 10 min is used in the numerical integration of the system of equations. The vertical discretization scheme is implicit, to avoid computational instabilities due to small grid spacing and relatively large time steps. The computational mode of solutions associated with the use of leapfrog time differencing is prevented by applying the Aselin filter at each time step.

[8] The physical model is initialized by stably stratified upper ocean temperature and salinity profiles representative of autumn conditions for the interior, i.e., cyclonic part of the sea. The biogeochemical model is initialized by simple and idealized conditions. A vertically uniform nitrate concentration of 4.0 mmol m^{-3} is specified within the upper 50 m, decreasing linearly to zero at 125 m. Oxygen is initially set to 50 μM within the first 50 m, to 10 μM within the next 60 m (including the SOL), and then to zero farther below near the lower boundary of the model. Other state variables of the model are initialized by small constant values over the water column. Starting from such highly arbitrary initial conditions, the model builds up an almost realistic biogeochemical structure within the first year as a response to the boundary conditions and then

Table 3. Definition and Values of Some Model Parameters Used in Simulations

Parameter	Definition	Value
ϵ	detritus decomposition rate	0.10 d^{-1}
κ	fraction of detritus remineralization directly converted to ammonium	0.85
α_0, α_1, α_2	stoichiometric coefficients	8.6, 8.6, 0.8
α_3, α_4	stoichiometric coefficients	1.5, 2.0
R_O	half saturation constant in oxygen dependence function of aerobic remineralization and nitrification	10.0 μM
K_O	half saturation constant in oxygen dependence function of anaerobic remineralization[a]	2.0 μM
k_3	rate of ammonium oxidation by O_2	0.1 d^{-1}
k_4	rate of sulfide oxidation by O_2	0.05 $\mu M\ d^{-1}$
k_5	rate of sulfide oxidation by MnO_2	30 $\mu M\ d^{-1}$
k_6	rate of ammonium oxidation by MnO_2	1.0 $\mu M\ d^{-1}$
k_7	rate of dissolved manganese oxidation by nitrate	0.25 $\mu M\ d^{-1}$
k_8	rate of conversion of nitrogen gas into nitrate	0.25 d^{-1}

[a] When oxygen is depleted in the water column, decomposition of particulate matter occurs anaerobically by utilizing nitrate. It has a maximum rate at zero oxygen concentration and decreases gradually as the oxygen concentration increases.

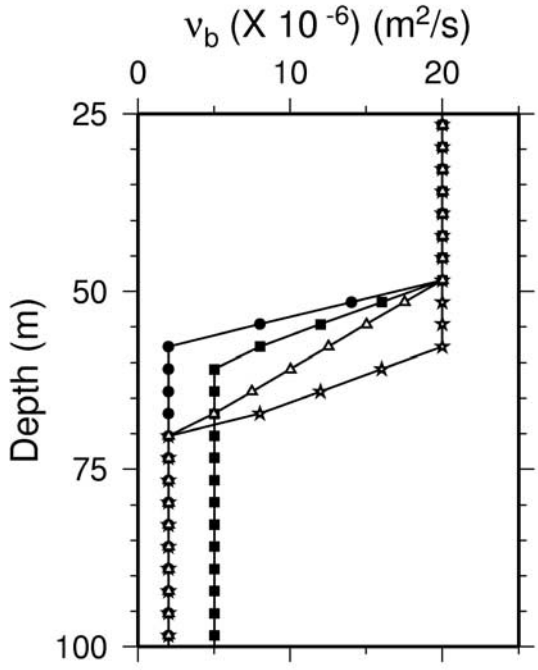

Figure 2. Different choices of depth profiles of the background vertical diffusion coefficient used in model simulations. Dots correspond to experiments A, B, and C; squares correspond to experiments D, E, and F; stars correspond to experiment CA; and triangles correspond to experiments CB and CC.

approaches an equilibrium state with yearly cycles of the upper layer physical and biogeochemical structures during the next 2 years of integration. The solutions described in section 3 are based on the fourth year of integration.

3. Model Experiments and Data Analyses

[9] The experiments presented in this section deal with the period of the *Aurelia*-dominated, highly eutrophic Black Sea ecosystem in the 1980s. This period includes the 1988 *Knorr* surveys during which the SOL structure was detected for the first time. Its ecosystem characteristics were recently modeled and validated by the data [*Oguz et al.*, 2000; 2001b]. We use this model to investigate the characteristics of the SOL as the response to organic matter production and recycling as well as to advective and diffusive oxygen supply across the oxycline. We consider different combinations of the vertical diffusion and velocity rates representing, in an idealized way, the cyclonic and anticyclonic flow regimes of the circulation. The vertical advection term is included for the equations of oxygen, hydrogen sulfide, nitrate, ammonium, and nitrogen gas. It is also included in the temperature and salinity equations of the physical model, in order to incorporate differences in the vertical density structure between cyclonic and anticyclonic flow regimes. However, it is not incorporated for the equations of the food web model, since the timescales of the biological processes are much faster (weekly) than those of the vertical advective processes (typically, monthly and seasonal). We also do not wish to introduce an additional complexity into the model that is not essential and directly relevant to the problem under consideration. For the same reason, we choose, in equation (3), a constant value of 3.0 m d^{-1} for the piston velocity. This is an optimum value estimated by our preliminary computations using its more complex parameterization depending on the wind speed. This choice of constant V_p is capable of providing a realistic range of summer-to-winter oxygen variations near the free surface [see *Oguz et al.*, 2000]. The suboxic layer dynamics therefore do not depend critically on the parameterization of the piston velocity.

[10] There are various estimates for the values of upwelling velocity and vertical diffusivity within the pycnocline waters of the Black Sea. Using box model calculation for the basin, *Murray* [1991] estimated w to be $\sim$1.0 cm d^{-1}. A similar estimate of 3.0 cm d^{-1} was given by *Samadurov and Ivanov* [1998]. The background value of vertical diffusivity, ν_b, within pycnocline waters of the southwestern Black Sea was measured by *Gregg and Ozsoy* [1999] to be around 1×10^{-6} m^2 s^{-1}. This value is consistent with estimations from empirically based formulae proposed by *Gargett* [1984] [see *Oguz et al.*, 2001b, Figure 2]. Similar values of w and ν_b were used by *Lewis and Landing* [1991] and provided reasonably realistic estimates of manganese oxidation rates.

[11] In these experiments, three values of w, as 4.0, 2.0, and -2.0 cm d^{-1}, are specified between depths of 25 and 125 m. Its value then decreases linearly to zero toward the surface and the bottom in order to avoid any advective source and sink across the boundaries. Vertical advection thus serves only for redistribution of the properties within the water column. The positive choices of w represent strong and moderate cyclonic flow conditions, whereas the negative value applies in a moderate anticyclonic case. These choices of w are accompanied by two different values of ν_b, as 2.0 and 5.0×10^{-6} m^2 s^{-1}, at depths corresponding to the oxycline and suboxic layers of the water column.

Table 4. Model Experiments

Experiment	w($\times 10^{-2}$), m d^{-1}	ν_b($\times 10^{-6}$), m^2 s^{-1}	Main Feature of Experiment
Experiment A	4.0	2.0	ν_b decreases linearly from 50 to 60 m
Experiment B	−2.0	2.0	ν_b decreases linearly from 50 to 60 m
Experiment C	2.0	2.0	ν_b decreases linearly from 50 to 60 m
Experiment CA	2.0	2.0	ν_b decreases linearly from 60 to 70 m
Experiment CB	2.0	2.0	ν_b decreases linearly from 50 to 70 m
Experiment CC	2.0	2.0	ν_b decreases linearly from 50 to 70 m
Experiment D	2.0	5.0	ν_b decreases linearly from 50 to 60 m
Experiment E	−2.0	5.0	ν_b decreases linearly from 50 to 60 m
Experiment F	4.0	5.0	ν_b decreases linearly from 50 to 60 m
Experiment CX	2.0	2.0	no biological sink terms in experiment C
Experiment CY	2.0	2.0	no biological source terms in experiment C
Experiment CZ	2.0	2.0	no vertical diffusion and advection terms in experiment C
Experiment GA	2.0	2.0	1.0-μM initial nitrate concentration in experiment C

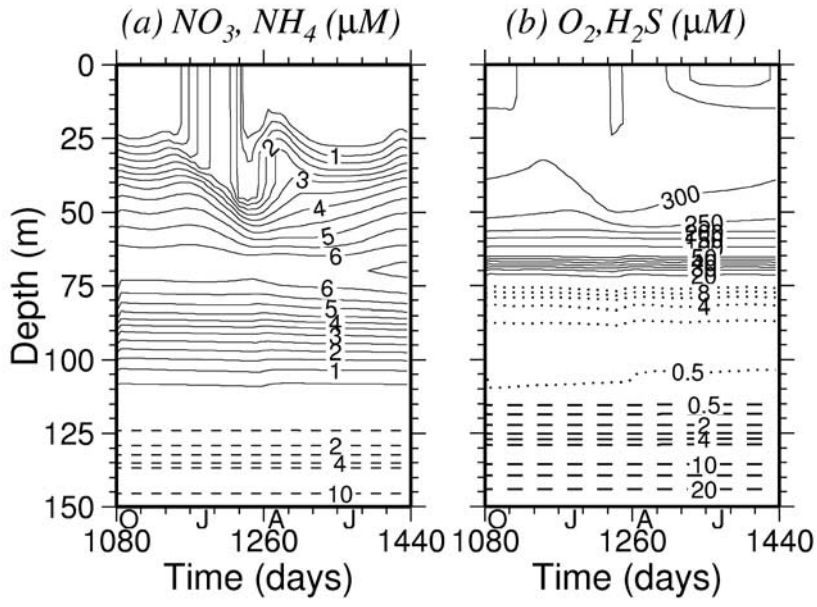

Figure 3. Fourth year, equilibrium solutions of water column (a) nitrate (solid lines) and ammonium (dashed lines) and (b) oxygen (solid and dotted lines) and hydrogen sulfide (dashed lines) for the standard experiment. Contours are given in units of μM at an interval of, for nitrate, 0.5 and, for ammonium, at an interval of 5 for concentrations from 10 to 5 and at an interval of 1 afterward. For oxygen concentration, contours are plotted at an interval of 50 (solid lines) for concentrations greater than 50, at 10 for concentrations from 50 to 10 (solid lines), and at 1 for concentrations of <10 (dotted lines). Hydrogen sulfide concentration contours are drawn at intervals of 5 for concentrations from 25 to 5 and at intervals of 0.5 for concentrations of <5. Time axis starts at 1 October and ends at 30 September.

[12] These uniform subsurface values of ν_b are increased linearly across the upper pycnocline zone (i.e., 50–75 m) to a value of 2.0×10^{-5} m^2 s^{-1} at 50 m and are kept constant at this value up to the surface (Figure 2), so that this value simulates the effects of stronger turbulence within the surface layer. This structure of ν_b is consistent with the one derived empirically using *Gargett*'s [1984] approach (shown by *Oguz et al.*, 2001a, Figure 2). Because our preliminary experiments showed that the equilibrium structure of the SOL depends on the way in which this transition is represented, we perform experiments using three different transition structures; ν_b varies linearly from 50 to 60 m in the first case (curve with dots in Figure 2), from 60 to 70 m in the second case (curve with stars in Figure 2), and from 50 to 70 m in the third case (curve with triangles in Figure 2).

[13] The experiments included here using different choices of the vertical diffusion and advection rate specifications are listed in Table 4. The one denoted by experiment C is referred to as the "main or standard experiment," reflecting a typical interior basin biogeochemical structure governed by a moderately strong cyclonic circulation regime. We first describe general characteristics of the vertical biogeochemical structure for such conditions (section 3.1) and then present its possible variations under different forms of vertical advection and diffusion as well as under different intensities of atmospheric cooling (sections 3.2 and 3.3).

3.1. General Characteristics of the Overall Biogeochemical Structure

[14] Starting from the initial conditions, transient adjustment of the solution is completed by the end of the second year, and the model provides similar yearly cycles of the properties for the third and fourth years. The equilibrium states of nitrate and ammonium as well as of dissolved oxygen and hydrogen sulfide distributions are shown in Figure 3. The vertical uniformity of the nitrate structure near the surface during the cold part of the year (Figure 3a) corresponds to the mixed layer deepening phase associated with intense vertical mixing in winter. Nitrate concentrations of $\sim$0.5 mmol m^{-3} within the upper 25 m during the autumn increase gradually to 1.5–2.0 mmol m^{-3} in February over a 50-m layer.

[15] At the beginning of March, there is a sudden and pronounced reduction in mixed layer nitrate concentrations due to consumption by phytoplankton production. During the warm period of the year the upper 25-m layer is depleted in nitrate to concentrations of <0.5 mmol m^{-3}. Nutrient recycling following the intense bloom events in March–April gives rise to a broader nitracline zone, where the nitrate accumulated is partially used to support the subsurface phytoplankton production in the late spring—early summer. The nitracline shoals and is gradually eroded during autumn when the mixed layer begins to entrain nitrate more actively from below, and nitrogen cycling accumulates some nitrate in the subsurface levels below the nitracline. The nitracline varies by $\sim$15 m during the annual cycle.

[16] The nitrate concentration below the maximum concentration zone remains unchanged throughout the year and decreases linearly by $\sim$4.0 mmol m^{-3} over a depth of $\sim$30 m. This zone is referred to as the lower nitracline and, as shown in Figure 3b, coincides with the suboxic zone characterized by oxygen concentrations of <10 μM. Ammonium prescribed at the

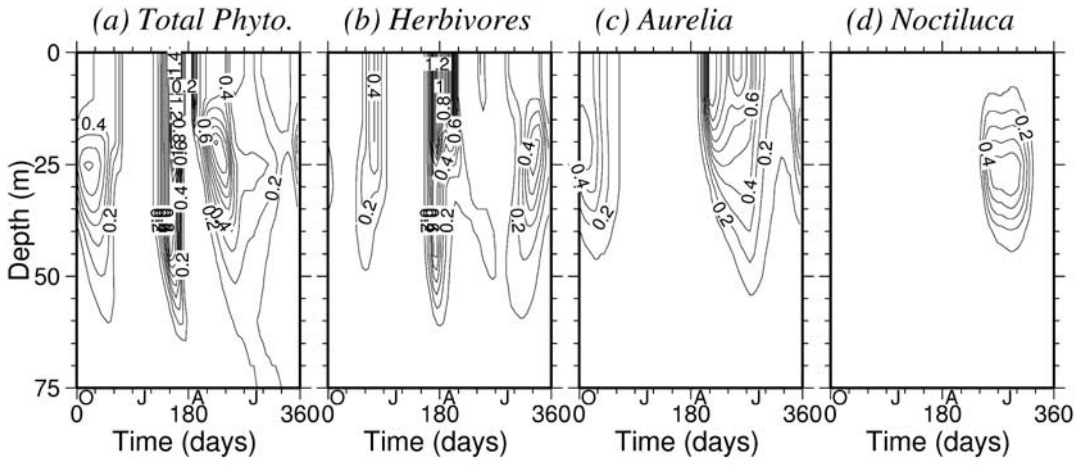

Figure 4. Annual distributions of (a) total phytoplankton (i.e., diatoms plus phytoflagellates), (b) total herbivores (microzooplankton plus mesozooplankton), (c) *Aurelia*, and (d) *Noctiluca* biomass computed from the standard experiment representing the ecosystem conditions of the late 1970s and 1980s during the period of intense eutrophication in the Black Sea. Units are in mmol N m^{-3}. Contours are drawn at an interval of 0.1 for all plots.

bottom boundary of the model diffuses and upwells toward the suboxic-anoxic interface (Figure 3a), where it is lost continually in the form of nitrogen gas due to its oxidation by particulate manganese. The suboxic-anoxic interface zone acts as a nutrient sink for the subsurface ammonium pool, which therefore cannot support new biological production in the euphotic zone [*Murray et al.*, 1995].

[17] Simulation of the subsurface nitrate maximum zone with peak concentrations of ~6 μM illustrates how efficiently the model provides a realistic nutrient recycling mechanism in the upper 75 m of the water column. Even though a vertically uniform nitrate profile is initially assigned, the model tends to generate a zone of maximum nitrate concentrations sandwiched between the losses on both sides due to phytoplankton uptake (above) and denitrification (below). The slight underestimation of peak nitrate concentrations compared with observed values of ~6–9 μM is probably due to the idealized specification of the initial nitrate profile and to the limitation of the present 1-D model for including the contribution of anthropogenic-based lateral nitrate supply that, in the long run, tends to contribute to the subsurface nitrate stocks of the entire basin. More details on the characteristics of nutrient cycling have been provided, using the same model, by *Oguz et al.* [2000].

[18] The oxygen concentrations specified initially as 50 μM within the euphotic zone and 10 μM within the suboxic layer respond quickly to the upper layer biogeochemical and physical characteristics of the system during the first year. Oxygen acquires a stable vertical structure within the euphotic zone by the second year, whereas the suboxic layer approaches an equilibrium by the third year. The SOL initially loaded with 10 μM oxygen concentration is gradually depleted in oxygen during the transient adjustment phase of the solutions. The mixed layer oxygen concentrations vary between 300 and 350 μM, with higher values during the winter and early spring due to the contribution of surface flux and photosynthetic production during these seasons (Figure 3b). Oxygen concentrations near the surface decrease by ~100 μM as a result of the flux to the atmosphere later in the summer months. All of these properties of the oxygen structure in the euphotic zone are consistent with observations [see *Oguz et al.*, 2000, Figure 12]. The oxycline is characterized by changes in oxygen concentration of 200–250 μM over a thickness of ~25 m, decreasing to a 10 μM value at 75 m. At greater depths the water column contains no appreciable dissolved oxygen concentrations. The suboxic zone has a temporally uniform structure and remains unaffected by seasonal variations of the surface layer oxygen structure.

[19] Evolution of the hydrogen sulfide structure within the anoxic layer responds to a source (25 μM) prescribed at the lower boundary of the model (Figure 3b). Steady state is approached by the end of the first year, with an upper boundary of hydrogen sulfide at ~100 m. This simulation using the particular choices of the vertical diffusion and upwelling velocity structures listed in Table 4 as experiment C (the standard experiment) thus reveals a nonsulfidic and oxygen-deficient suboxic zone of ~40 m, between the depths of 75 and 115 m. This structure resembles quite favorably those given by the observations [*Friederich et al.*, 1990; *Murray*, 1991; *Codispoti et al.*, 1991; *Tugrul et al.*, 1992; *Saydam et al.*, 1993; *Buesseler et al.*, 1994; *Basturk et al.*, 1994, 1997; *Oguz et al.*, 2001a; *Konovalov and Murray*, 2001].

[20] Before proceeding further on the details of the suboxic zone structure, it is appropriate to briefly describe the equilibrium characteristics of the euphotic zone biology, which constitutes one of the factors governing suboxic layer characteristics. The total phytoplankton (i.e., the sum of diatoms and phytoflagellates), total herbivores (i.e., the sum of microzooplankton and mesozooplankton), *Aurelia*, and *Noctiluca* biomass distributions over the year are shown in Figure 4. The total phytoplankton biomass (Figure 4a) reflects the most intense bloom event of the year, starting from about the second half of February to the second week of March. The bloom extension over the entire mixed layer of ~50 m reflects its formation before termination of winter mixing. Following a 2-week recycling period, a second phytoplankton bloom episode starts in a shallower mixed layer of ~20 m in April and then shifts in May–June to subsurface levels, which have already accumulated a considerable amount of recycled nitrogen (Figure 3a). This second bloom is terminated

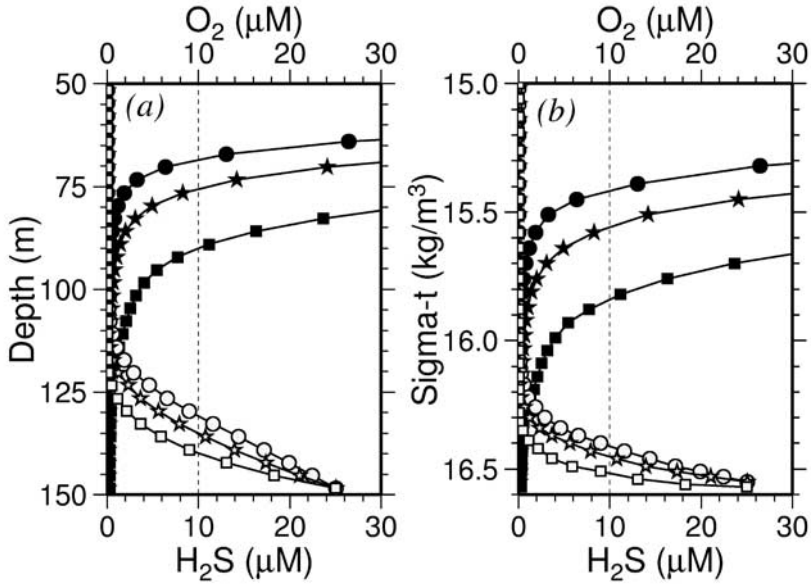

Figure 5. Annual mean profiles of oxygen (solid symbols) and hydrogen sulfide (open symbols) plotted versus (a) depth and (b) σ_t for three different choices of vertical velocity for 4.0 cm d^{-1} (strong upwelling case (circles)), 2.0 cm d^{-1} (moderate upwelling case (stars)), and -2.0 cm d^{-1} (moderate downwelling case (squares)). Background value of the vertical diffusion coefficient at subsurface levels is 2.0×10^{-6} m^2 s^{-1}.

by mid-July and is followed by a third phytoplankton production event during October–November.

[21] Total herbivore biomass (Figure 4b) follows the phytoplankton activity closely during the year. *Aurelia* biomasses are highest in the summer and acquire a secondary peak during the early autumn period (Figure 4c). *Noctiluca* growth is limited to only the summer months (Figure 4d). Further details on the annual plankton structure, interactions between different planktonic groups, and consistency of the model simulation with the data are presented by *Oguz et al.* [2000, 2001b]. The important point to emphasize here is the presence of year-long enhanced biological activity in the euphotic zone, providing an almost continuous supply of organic matter to deeper levels of the water column.

3.2. How is the SOL Structure Controlled by Vertical Advection and Diffusion?

3.2.1. Simulations for cyclonic and anticyclonic regimes of basin circulation. [22] Annual mean profiles of dissolved oxygen and hydrogen sulfide concentrations for two different values of the background vertical diffusivity are shown in Figures 5 and 6. Each of them also includes three different choices of vertical velocity, while the rest of the parameters are identical. In Figure 5, experiment A corresponds to the case of w = 4.0 cm d^{-1} and ν_b = 0.02 cm^2 s^{-1}. It illustrates that the combination of strong upwelling and weaker diffusion is the most favorable condition for the formation and maintenance of the SOL. When the upwelling velocity is weaker (2.0 cm d^{-1}), experiment C provides the distributions presented in Figure 3b. These two cases represent conditions within the cyclonically dominated interior parts of the basin surrounded by a narrow peripheral zone of anticyclonic eddies and meandering Rim Current structure. These upwelling experiments can be compared with downward vertical velocity of $w = -2.0$ cm d^{-1} (experiment B), as expected for moderate anticyclones.

[23] Upwelling is a crucially important factor governing the structure of the suboxic layer (Figure 5). While the SOL has a thickness of ~20–40 m for all values of upwelling, the SOL itself is located at different depths with different thicknesses. In the first two cases with upwelling, the SOL lies between 70 and 110 m for experiment A (corresponding to σ_t of ~15.40 and ~16.20 kg m^{-3}) and lies between 75 and 115 m for experiment C (corresponding to σ_t of ~15.60 and ~16.20 kg m^{-3}). Oxygen has a limited penetration toward the anoxic interface, and the lower boundary of the SOL is controlled predominantly by oxidation of sulfide with particulate manganese produced by nitrate-based reactions. In the third case, for experiment B, the presence of downwelling velocity results in penetration of dissolved oxygen to deeper levels, as shown by the position of the upper boundary of SOL at ~90 m (σ_t of ~15.85 kg m^{-3}). The absence of upward vertical velocity for this case implies more limited hydrogen sulfide transported toward the interface zone by means of vertical diffusion only. Conversely, the nonzero downward velocity allows penetration of more oxygen toward deeper levels. Thus sulfide oxidation takes place up to a depth of 125 m at σ_t of ~16.30 kg m^{-3}, and the SOL attains a narrower thickness as compared with cyclones.

[24] The annual mean oxygen and sulfide profiles using a higher diffusion rate in subsurface levels (ν_b = 0.05 cm^2 s^{-1}) are shown in Figure 6. For cyclonic cases, the position of the lower boundary of the SOL remains the same, but the upper boundary deepens by ~10 m relative to the corresponding cases in Figure 5. The thickness of the SOL thus decreases to ~30 m for both experiment F (moderate cyclone) and experiment D (weak cyclone). For experiment E (strong anticyclone), the SOL is narrower, and its boundaries are identified at 110 and 130 m. The presence of higher diffusion results in stronger downward diffusive transport of oxygen, which somewhat counters the effect of upwelling flux and gives rise to a relatively shallower and deeper SOL as compared to those shown in Figure 5. The most extreme case is the combination

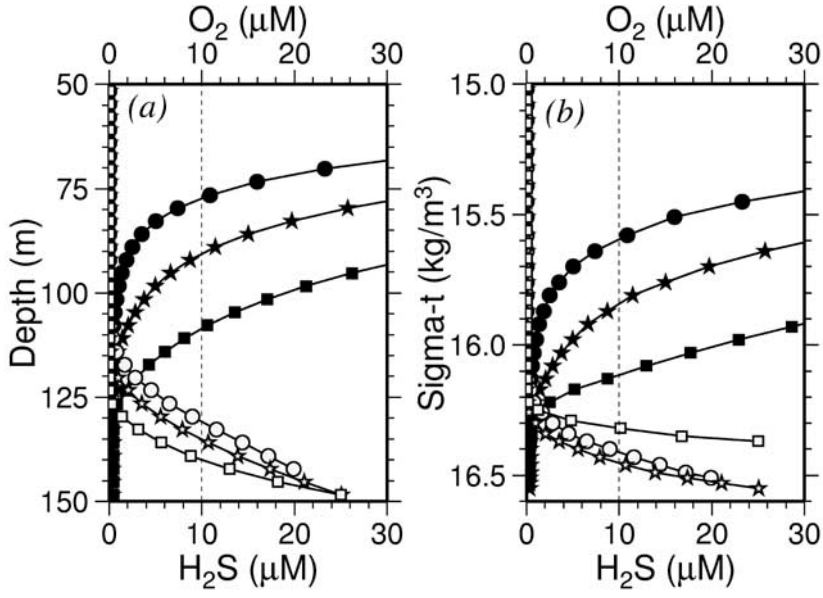

Figure 6. Same as in Figure 5, but for subsurface value of the background vertical diffusion coefficient of 5.0×10^{-6} m^2 s^{-1}.

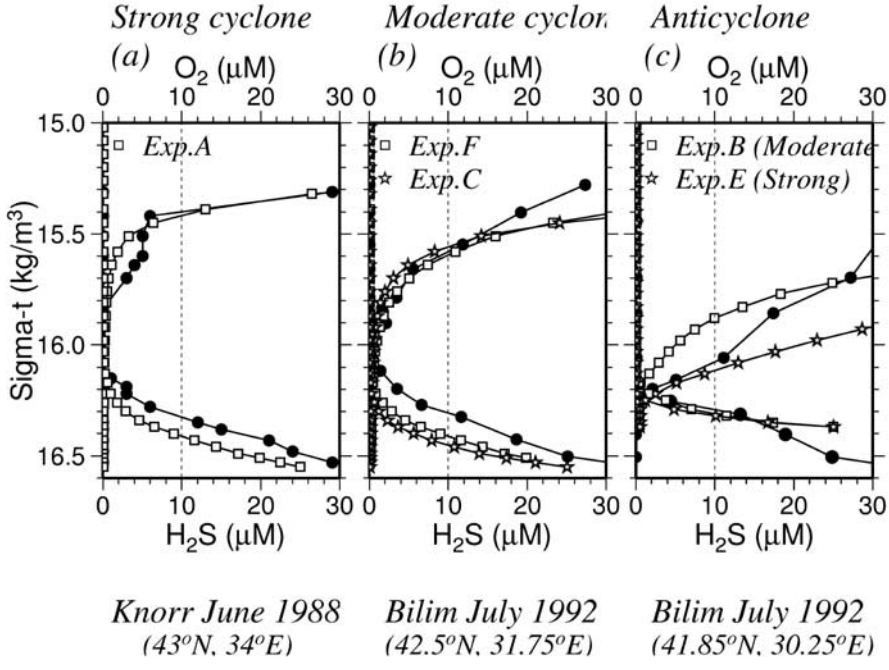

Figure 7. Dissolved oxygen and hydrogen sulfide profiles against σ_t (kg m^{-3}). Solid circles represent observations, whereas squares and stars represent annual mean profiles computed from the model for different combinations of vertical velocity and background diffusion coefficient. Curves in the upper part of each plot correspond to oxygen, and curves in the lower part correspond to hydrogen sulfide.

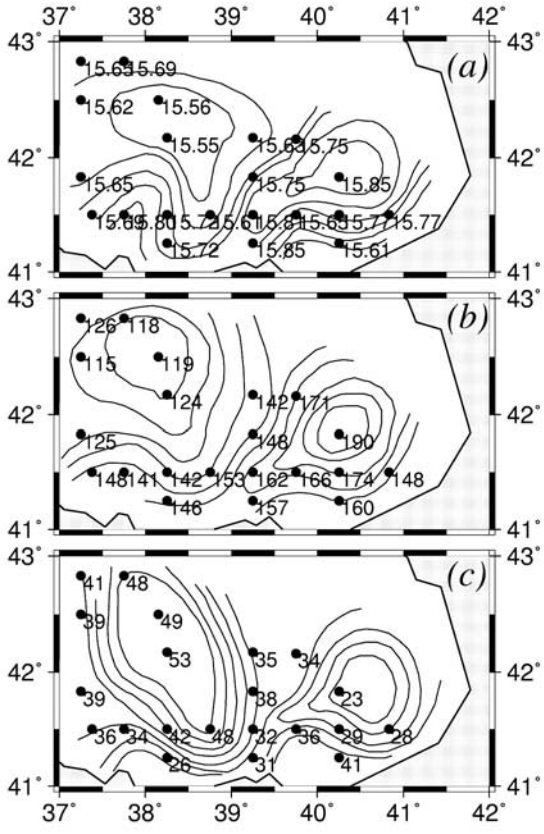

Figure 8. Horizontal distributions of (a) σ_t (kg m^{-3}) at the depth of 10 μM oxygen concentration and (b) at the depth of 10 μM oxygen concentration and (c) thickness of the SOL obtained from measurements of the R.V. *Bilim* 1991 survey in the southeastern part of the Black Sea. SOL thickness is defined by the difference between depths of $\sigma_t \approx 16.2$ kg m^{-3} (lower boundary) and of the 10 μM oxygen concentration (upper boundary). Station locations are shown by dots. Actual measured values are also indicated.

of strong diffusion and downwelling (i.e., strong anticyclone), in which the SOL thickness is ~20 m.

[25] The annual mean oxygen profiles for these experiments plotted against density (Figure 7) agree with observed profiles chosen from distinctly different sites in the Black Sea with different circulation regimes. For the strong cyclonic flow regime (Figure 7a), the boundaries of the SOL lie at σ_t of ~15.40 and ~16.20 kg m^{-3}. It is illustrated fairly well by the profile taken at the central part of the Black Sea cyclonic gyre (43°N, 34°E) during the *Knorr* cruise in June 1988. This is a more atypical and extreme case, and only a few such profiles were found within the entire R.V. *Bilim* data set comprising the measurements from the 1990s. Figure 7b, indicating the moderate cyclonic case given by the simulations experiment C (Figure 5) and experiment F (Figure 6), suggests SOL boundaries of σ_t of ~15.60 and ~16.20 kg m^{-3}. It reflects a more typical structure within the interior Black Sea waters, as shown by observed profiles from the interior of the western cyclonic gyre (42.5°N, 31.75°E).

[26] The observational support for the SOL structure in the anticyclonic flow regime in Figure 7c is provided by a measurement during July 1992 at a station inside the quasipermanent Sakarya anticyclonic eddy along the Anatolian coast, east of the Bosphorus (41.85°N, 30.25°E). This case represents a limiting case of the suboxic layer with oxygen concentrations of >50 μM at $\sigma_t \approx 15.5$ kg m^{-3}, reducing to the 10 μM level only at $\sigma_t \approx 15.85$ kg m^{-3} for the moderate anticyclone and $\sigma_t \approx 16.10$ kg m^{-3} for a more extreme case of a strong anticyclone. The observed profile lies between these two anticyclonic simulations. The lower boundary of the SOL coincides with $\sigma_t \approx 16.25$ kg m^{-3}.

[27] The simulated and measured oxygen profiles shown in Figure 7 do not suggest isopycnal uniformity of the SOL properties independent of the circulation and physical characteristics. On the contrary, they clearly provide a direct and one-to-one correspondence with the circulation. This result is further supported in Figure 8 by the additional data from R.V. *Bilim* 1991 oxygen measurements from the southeastern part of the basin, where the circulation is characterized by a dual gyre system (i.e., a combination of cyclone and anticyclone) and the Rim Current jet zone in between [see *Oguz et al.*, 1994, Figure 4]. The anticyclonic gyre is situated east of the Rim Current zone and is known to be the Batumi eddy. The cyclonic gyre is located on the western flank of the Rim Current jet and constitutes a member of the eastern basin interior cyclonic circulation. Therefore this system, covered by a fairly dense set of stations of oxygen and sulfide measurements, is an ideal combination to test the dependence of the SOL properties on circulation characteristics. The density distribution at the depth of 10 μM oxygen concentration (i.e., the position of the upper boundary of the SOL in terms of density) is shown in Figure 8a, and the same distribution with respect to depth is shown in Figure 8b. Figure 8c, conversely, illustrates the horizontal variability of the SOL thickness with respect to a 16.2 kg m^{-3} reference density level taken as its lower boundary.

[28] They all provide a remarkable agreement between the circulation features and the SOL properties. While the upper SOL boundary is characterized by $\sigma_t \approx 15.55$ kg m^{-3} at the center of the cyclonic gyre, it is identified by a $\sigma_t \approx 15.85$ kg m^{-3} level within the Batumi anticyclone, with significant changes within the narrow Rim Current transition zone in between (Figure 8a). Regionally, there is almost a 100% contrast in the depth of the upper SOL boundary (~75 versus 165 m) and in the SOL thickness (~50 versus 25 m) of these two gyres. The model-simulated hydrogen sulfide profiles, conversely, differ consistently from those observed. Contrary to different structures of sulfide profiles depending on the values of diffusion coefficient and vertical velocity, the observations suggest a more uniform structure decaying with a similar slope toward $\sigma_t \approx 16.20$ kg m^{-3}. This difference suggests a more active control of biogeochemical processes on the anoxic interface structure as compared to their physical counterparts. The biogeochemical model formulation can only provide first-order characteristic features of the anoxic interface structure, and a more sophisticated formulation appears to be necessary for a more realistic prediction. This is, however, beyond the scope of the present study.

3.2.2. Effect of different types of background diffusivity structure within the oxycline region. [29] In addition to values of vertical diffusivity and upwelling velocity, we now show how the position of the upper boundary of the SOL is sensitive to small hanges in the linearly varying portion of ν_b. The simulations using the four different profiles shown in Figure 2 are designated by experiment C, experiment D, experiment CA, and experiment CB in Table 4. The corresponding annual mean dissolved oxygen profiles are plotted against density in Figure 9. The profiles shown by circles and squares represent the cases for experiments C and D, respectively. They clearly show how the change in the magnitude of the subsurface diffusivity within the oxycline and the SOL from 0.02 to 0.05 cm^2 s^{-1} leads to a higher rate of oxygen supply into the SOL and deepens its upper boundary by $\Delta\sigma_t \approx 0.25$ kg m^{-3}.

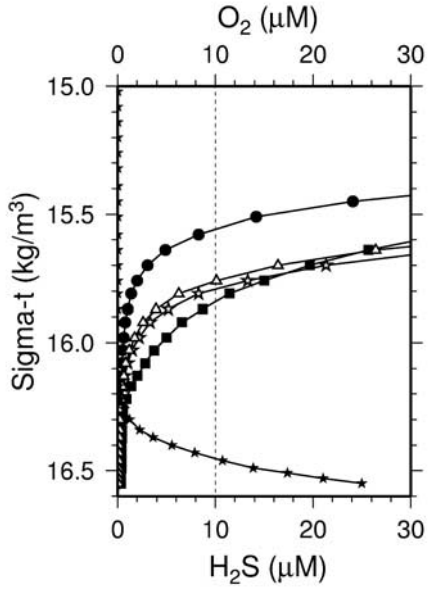

Figure 9. Annual mean profiles of oxygen and hydrogen sulfide plotted versus σ_t for different choices of background vertical diffusion coefficient. Profile with solid circles corresponds to experiment C, squares correspond to experiment D, stars correspond to experiment CA, and triangles correspond to experiment CB. Curves in upper part of each plot correspond to oxygen, and curves in lower part correspond to hydrogen sulfide.

The simulations shown by the triangles and stars represent the cases where the linear transition is altered slightly from its original 10-m range, between 50 and 60 m depth, to either 50–70 m (steeper slope; experiment CB), or to 60–70 m (experiment CA). Both of these slight changes exert higher rates of oxygen transport across the transition zone immediately below the biologically and atmospherically maintained high oxygen concentration zone and consequently lead to a deepening of the upper SOL boundary of almost $\Delta\sigma_t \approx 0.2$ kg m^{-3}, or ~20 m.

[30] Although each of these profiles represents a steady state solution for a particular ν_b structure, they may be quite instructive for understanding and interpreting the impact of temporal variability in small-scale mixing characteristics within the oxycline region over the course of a year. For example, the 1988 *Knorr* data set comprises a set of measurements at 43°N, 34°E, which is a site at the center of the narrowest section of the Black Sea, between the tip of Crimea on the north and Cape Sinop on the south. The physical and chemical measurements were repeated five times during a 1.5-month period between 13 June and 25 July 1988. The profiles of density and oxygen versus depth (Figures 10a and 10b) demonstrate remarkably well how changes in the circulation and stratification characteristics on a weekly basis can induce considerable modifications in the density structure of the upper pycnocline and the slope of oxycline and, therefore, in oxygen concentrations of the oxycline zone.

[31] Comparison of the density profiles for 13 June (solid circles) and 29 June (solid squares) reveals a decrease in the density of subsurface waters (Figure 10a). For example, the density at 60 m decreased from $\sigma_t \approx 15.05$ to $\sigma_t \approx 14.85$ kg m^{-3} during this period. This change was due to temperature changes from 7.20° to 6.97°C and due to salinity changes from 19.28 to 18.98, implying a downward supply of water from the central part of the overlying Cold Intermediate Layer. The oxygen concentration increased considerably within the transition zone as well, as reflected by a change from 50 to 190 μM at 60 m (Figure 10b). The subsequent three casts (shown by stars for 18 July, triangles for 21 July, and circles for 25 July) demonstrate an opposite and upwelling-type flow regime, as suggested by a persistent increase in the density and reduction in oxygen concentrations. For example, the density at 60 m increases to $\sigma_t \approx 15.15$ kg m^{-3} within a month as a result of a supply of slightly warmer (temperature increasing to 7.32°C) but more saline (salinity increasing to 19.36) water from farther below. Upwelling of less oxygenated waters also causes an almost 50% decrease in the oxygen concentrations

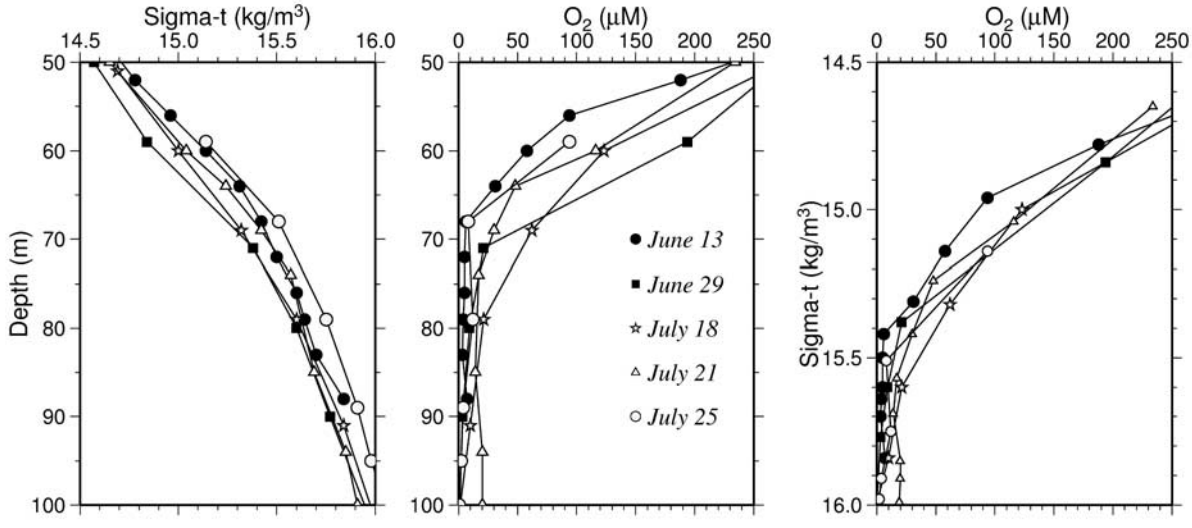

Figure 10. Profiles of (a) density (in σ_t (kg m^{-3})), (b) oxygen (μM) plotted against depth, and (c) oxygen (μM) plotted against σ_t (kg m^{-3}) at station 43°N, 34°E, measured at different casts during 13 June through 25 July *Knorr* 1988 survey.

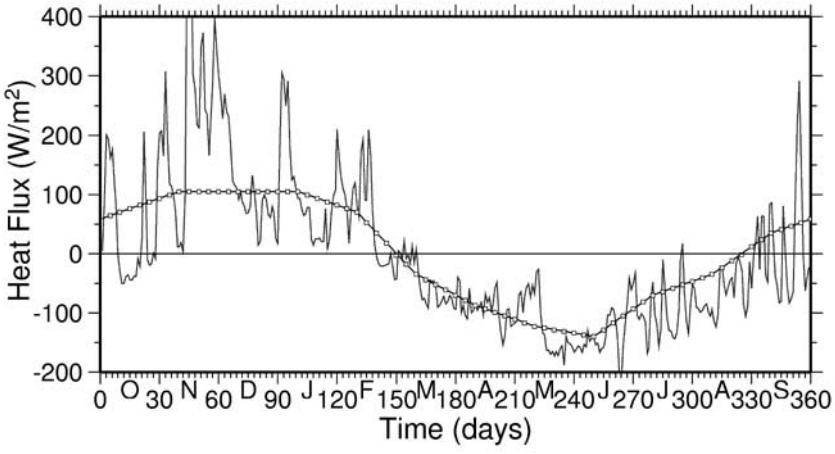

Figure 11. Daily heat flux variations used in the model. The smooth curve with circles represents the climatologically mean annual distribution, whereas the solid line corresponds to that of year 1993, which is one of the coldest years in the last decade. Time axis starts at 1 October and ends at 30 September.

within the oxycline, as implied by its reduction to ~100 μM at 60 m.

[32] The oxygen versus density profiles (Figure 10c) also show similar changes in the oxygen concentrations. However, the important point we wish to draw attention to here is that it will not be enough, by itself, to understand and interpret how these changes took place in the water column without looking at the water mass characteristics. In the absence of depth versus density profiles (i.e., without plotting Figure 10a), temporal changes observed in the oxygen concentrations in Figure 10c may be explained entirely from a biogeochemical point of view, i.e., by a scenario based on oxygen production/consumption. Conversely, if they are interpreted in the light of knowledge about the water mass characteristics (i.e., Figure 10a), an alternative and realistic explanation based on their dependence on the vertical physical processes may be provided to explain changes in the oxygen concentrations.

[33] It is also appropriate to describe here an episode of short-term changes in the oxygen concentration near the base of the SOL during 21 and 25 July. The 21 July oxygen profiles shown in Figures 10b and 10c suggest an increase of oxygen concentration up to ~26 μM around ~100 ± 10 m and around $\sigma_t \approx 16.00 \pm 0.1$ kg m^{-3} level. This implies lateral injection of oxygen from either the southern or northern coastal zones associated possibly with a Rim Current meander, as shown by the numerous hydrographic and satellite-based (advanced very high resolution radiometer (AVHRR), Sea-viewing Wide Field-of-view Sensor (SeaWiFS), and altimeter) studies on the mesoscale-dominated circulation of the Black Sea. The 25 July profile suggests that this additional oxygen is consumed immediately, and the suboxic layer is identified once again by concentrations of <10 μM. The lateral injection of oxygen and associated onshore-offshore interactions of oxygen between the shelf and interior waters around the periphery of the basin is a well-known feature of the Black Sea and has been noted in many different studies [e.g., *Oguz et al.,* 1991; *Ozsoy et al.*, 1993; *Basturk et al.*, 1998; *Oguz et al.*, 2001a].

3.3. Is It Possible to Ventilate the Suboxic Zone by Atmospheric Oxygen Input?

[34] The experiments described in sections 3.1 and 3.2 involve specification of a smooth climatological daily heat flux distribution without variations on weekly timescales associated with pulses of cold air outbreaks. It is therefore of interest to examine whether imposition of stronger cooling could lead to a denser water mass formation, and subsequently to deeper penetration of the winter mixed layer, and thus to a higher rate of oxygen supply to deeper levels, including the suboxic layer. The standard experiment (experiment C) is repeated using the daily heat flux data for the year 1993, which included one of the strongest winters of the last decade in the region. When compared with the climatological mean daily heat flux data of the standard experiment (shown by the smooth curve with circles in Figure 11), it shows a series of strong episodic cooling events, each of which lasts about a week during the autumn and winter months (shown by the continuous line in Figure 11). Each of these episodic events typically imposes more than 200 W m^{-2} higher cooling as compared to the climatological case. In another experiment these particular heat flux data are made even stronger by increasing the values by 50% so that they represent a case of exceptionally strong and cold winter.

[35] The first point that can be noted in these experiments is the temporal uniformity of the density and oxygen structures below ~50 m throughout the year, as in the standard case. The oxycline and suboxic zone are decoupled completely from the atmospherically induced fluctuations in the surface layer. The second finding is the presence of negligible change in the subsurface density and oxygen structures, even for the exceptionally strong cooling case (Figure 12a). At 50 m the density increases by ~0.2 kg m^{-3} (from 15.08 to 15.27 kg m^{-3}), whereas oxygen concentration changes slightly from 258 to 270 μM. At 75 m the changes are even smaller, and the density value of $\sigma_t \approx 15.58$ kg m^{-3} of the standard experiment increases to only $\sigma_t \approx 15.71$ kg m^{-3}, whereas oxygen concentrations remain around 8.0 μM for both cases. Therefore the depth of 10 μM oxygen concentration does not change (Figure 12b) because of the lack of ventilation of the suboxic zone, even though the density at this depth is increased as a result of the change in the water column stratification characteristics. When the oxygen profiles are plotted against density for the standard and strong cooling cases (Figure 12c), the upper boundary of the suboxic zone appears at a deeper density level. As shown in Figure 10, even if the profile merely indicates the presence of slightly denser water at the same depth

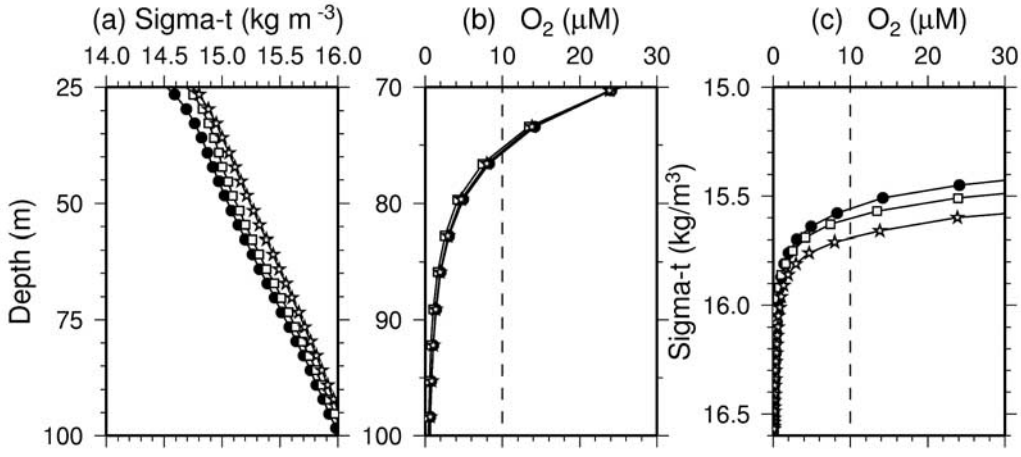

Figure 12. Annual mean profiles of (a) density (in σ_t (kg m^{-3})), (b) oxygen (μM) plotted against depth, and (c) oxygen (μM) plotted against σ_t (kg m^{-3}) for different heat flux forcings. Solid circles correspond to standard simulation with climatological heat flux, open circles correspond to standard simulation with the 1993 heat flux, and stars correspond to standard simulation with 50% stronger 1993 heat flux forcing.

level due to extra cooling, it may be interpreted as the deeper penetration of oxygen into the suboxic layer. This is another example showing the risk of defining biogeochemical properties in terms of preassigned density levels.

4. Summary and Concluding Remarks

[36] A prognostic, 1-D vertically resolved coupled physical-biogeochemical model is used to investigate the role of vertical physical processes for controlling the structure of the SOL in the Black Sea. This work is an extension of our previous study [*Oguz et al.*, 2000] involving specific food web, nitrogen cycle, and redox models describing the biogeochemical system of the oxic, suboxic, and anoxic waters of the interior Black Sea. The present model is specifically used to test the assumption of isopycnal homogeneity of the SOL properties and their independence from the circulation features, as proposed 10 years ago and generally assumed ever since. This assumption has never been verified convincingly by available data and/or supported by specific model simulations.

[37] The concept of isopycnal uniformity was originated when the composite oxygen, sulfide, and nutrient profiles were plotted against density by combining all the casts carried out during the 1988 *Knorr* surveys. Because the oxygen data from pumpcast measurements mostly belonged to stations from the interior part of the western and central basins [see *Codispoti et al.*, 1991, Figure 1] characterized by the same type of (i.e., cyclonic) circulation system, this approach worked rather well. This assumption, however, may not be uniformly valid when the composite is formed by pooling data from different parts of the basin with different circulation regimes. The cyclonic regions, in which the downward diffusive supply of oxygen into the suboxic zone is opposed by its upward advective flux, are expected to possess a somewhat different type of SOL structure as compared to anticyclones with more pronounced downward oxygen transport. Contrary to large-scale open ocean eddies, domination of the Black Sea circulation by highly energetic mesoscale eddy fields [*Korotaev et al.*, 2001] suggests a more pronounced role for the vertical processes in controlling the spatial structure of the suboxic layer. This is shown remarkably well by the data for a cyclonic-anticyclonic eddy pair on the eastern basin (see Figure 8). Our experiments with different combinations of upwelling/downwelling velocity and vertical diffusion coefficient cover all possible local conditions representing different regimes of this system uncoupled by the horizontal advective motions.

[38] For given parameter ranges of vertical velocity and diffusion coefficient, a series of experiments has been performed to cover the strong and moderate cyclonic and anticyclonic regimes and to cover a transition between these two representing the Rim Current zone. As expected, weaker diffusion and stronger upwelling provide the most favorable conditions for the formation of SOL within the interior cyclonic cell of the basin. It is found that while vertical diffusivity controls the position of the upper boundary of the SOL, the upwelling velocity primarily controls its lower boundary. Thus anticyclones, with downwelling and downward diffusion (and thus with stronger net downward supply of oxygen), attain a thinner SOL at a deeper part of the water column relative to cyclones, which are characterized by weaker net downward oxygen supply. These model findings agree quite well with observations and reveal a difference of $\sigma_t \approx 0.3$ kg m^{-3} in the thickness and upper boundary position of the SOL between cyclones and anticyclones. Its lower boundary is, conversely, relatively insensitive to the changes in the vertical physical characteristics. It is essentially governed by biogeochemical reactions and is identified by $\sigma_t \approx 16.15 \pm 0.05$ kg m^{-3}. We then conclude that the vertical physical processes are crucially important factors governing the basinwide distribution of the oxycline and SOL properties. This suggests that composite plots of oxygen versus density for cyclonic and anticyclonic sites should be constructed separately. If they are plotted together, as has been previously done, the profiles exhibit a great deal of scatter, especially in the SOL section. Such scatter has been falsely interpreted as sampling and measurement error in the past. Our analyses suggest that the quality of the R.V. *Bilim* data collected during the 1990s is better than previously believed and that the analytical error in these oxygen analyses does not exceed 5 μM.

[39] Another serious problem arises when oxygen versus density profiles from different data sets are compared with each other to reach conclusions regarding the temporal variability of the water column biogeochemical structure. Such a comparison implicitly

assumes that the density remains unchanged in all these measurements, and thus all variabilities are associated with biogeochemical processes. However, density of the water column is also subject to seasonal variabilities, and therefore each of these oxygen profiles, when plotted against density, includes some contribution from the change in the temperature and salinity characteristics. Therefore it may not be entirely appropriate to investigate temporal variability of the water column oxygen properties using the oxygen versus density profiles alone. Observational evidence for such a case was provided by five simultaneous oxygen measurements from the 1988 *Knorr* survey carried out at a station within the central part of the basin during a 1.5-month period from mid-June to the end of July. The water column had been first under the influence of downwelling motion, with subsequent reduction in density and increase in oxygen concentrations in the oxycline zone. This period was followed by a flow reversal, in which the water column was governed by upwelling motion, which gives rise to an increase in the density and reduction in oxygen concentrations of the oxycline zone. All of these changes in the density characteristics falsely emerge as short-term variabilities in the oxycline and the upper boundary of SOL when the depth variations in oxygen concentrations are expressed in terms of density.

[40] The Black Sea has a very strong density stratification changing from $\sigma_t \approx 10.0-11.0$ kg m^{-3} at the surface (in summer months) to $\sigma_t \approx 15.5$ kg m^{-3} at 75 m and $\sigma_t \approx 16.0$ kg m^{-3} at 100 m within the cyclonic interior basin. Even a series of exceptionally strong winter cooling episodes cannot make the water column dense enough (up to $\sigma_t \approx 15.5$ kg m^{-3}) to overturn and thus ventilate the SOL with the winter mixed layer oxygen concentrations of $\sim$350 μM. According to our simulations, the Black Sea can at most be ventilated up to 60 m, where the maximum density of the winter mixed layer is around $\sigma_t \approx 15.0$ kg m^{-3}. Therefore the SOL structure has no direct coupling with the physical and biogeochemical processes of the near-surface levels throughout the year. The link is indirect, physically, through diffusive supply for the major (i.e., cyclonic) part of the basin and is indirect, biogeochemically, through remineralization and nitrification losses.

[41] **Acknowledgments.** T. Oguz acknowledges support by NSF grant OCE-9906656 and by NATO Linkage grant EST. CLG975821. We thank J. Staneva for providing us with the 1993 daily heat flux data. This research is a contribution to the ODBMS Black Sea project sponsored by the NATO Science for Peace Program. The comments and thorough editing of the manuscript by J. Murray and J. Nevins were greatly appreciated. We also thank the reviewers (L. Codispoti and W. Reeburgh) for their comments.

References

Basturk, O., C. Saydam, I. Salihoglu, L. V. Eremeeva, S. K. Konovalov, A. Stoyanov, A. Dimitrov, A. Cociasu, L. Dorogan, and M. Altabet, Vertical variations in the principle chemical properties of the Black Sea in the autumn of 1991, *J. Mar. Chem.*, *45*, 149–165, 1994.

Basturk, O., S. Tugrul, S. Konovalov, and I. Salihoglu, Variations in the vertical structure of water chemistry within the three hydrodynamically different regions of the Black Sea, in *Sensitivity to Change: Black Sea, Baltic Sea and North Sea, NATO Sci. Partnership Subser. 2*, vol. 27, edited by E. Ozsoy and A. Mikaelyan, pp. 183–196, Kluwer Acad., Norwell, Mass., 1997.

Basturk, O., I. I. Volkov, S. Gokmen, H. Gungor, A. S. Romanov, and E. V. Yakushev, International expedition on board R/V *Bilim* in July 1997 in the Black Sea, *Oceanology, Engl. Transl.*, *38*, 429–432, 1998.

Buesseler, K. O., H. D. Livingston, L. Ivanov, and A. Romanov, Stability of the oxic-anoxic interface in the Black Sea, *Deep Sea Res., Part I*, *41*, 283–296, 1994.

Codispoti, L. A., G. E. Friederich, J. W. Murray, and C. M. Sakamoto, Chemical variability in the Black Sea: Implications of continuous vertical profiles that penetrated the oxic/anoxic interface,, *Deep Sea Res.*, *38*(Suppl. 2), S691–S710, 1991.

Friederich, G. E., L. A. Codispoti, and C. M. Sakamato, Bottle and pumpcast data from the Black Sea expedition, *Tech. Rep. 90-3*, 224 pp., Monterey Bay Aquarium Res. Inst., Moss Landing, Calif., 1990.

Gargett, A. E., Vertical eddy diffusivity in the ocean interior, *J. Mar. Res.*, *42*, 359–393, 1984.

Gregg, M. C., and E. Ozsoy, Mixing on the Black Sea shelf north of the Bosphorus, *Geophys. Res. Lett.*, *26*, 1869–1872, 1999.

Konovalov, S. K., and J. W. Murray, Variations in the chemistry of the Black Sea on a time scale of decades (1960–1995), *J. Mar. Syst.*, *31*, 217–243, 2001.

Korotaev, G. K., O. A. Saenko, and C. J. Koblinsky, Satellite altimetry observations of the Black Sea level, *J. Geophys. Res*, *106*, 917–933, 2001.

Lewis, B. L., and W. M. Landing, The biogeochemistry of manganese and iron in the Black Sea, *Deep Sea Res.*, *38*(Suppl. 2A), S773–S804, 1991.

Luther, G. W., III, B. Sundby, B. L. Lewis, P. J. Brendel, and N. Silverberg, The interaction of manganese with the nitrogen cycle in continental margin sediments: Alternative pathways for dinitrogen formation, *Geochim. Cosmochim. Acta*, *61*, 4043–4052, 1997.

Murray, J. W., Black Sea oceanography: Results from the 1988 Black Sea Expedition, *Deep Sea Res.*, *38*, Suppl. 2A, 1266 pp., 1991.

Murray, J. W., L. A. Codispoti, and G. E. Friederich, Oxidation-reduction environments: The suboxic zone in the Black Sea, in *Aquatic Chemistry: Interfacial and Interspecies Processes*, *ACS Adv. in Chem. Ser.*, vol. 224, edited by C. P. Huang, C. R. O'Melia, and J. J. Morgan, pp. 157–176, Am. Chem. Soc., Washington, D. C., 1995.

Murray, J. W., B.-S. Lee, J. Bullister, and G. W. Luther III, The suboxic zone of the Black Sea, in *Environmental Degradation of the Black Sea: Challenges and Remedies*, *NATO Sci. Partnership Subser. 2*, vol. 56, edited by S. T. Besiktepe, U. Unluata, and A. S. Bologa, pp. 75–91, Kluwer Acad., Norwell, Mass., 1999.

Oguz, T., et al., Mesoscale circulation and thermohaline structure of the Black Sea observed during HydroBlack '91, *Deep Sea Res., Part I*, *41*, 603–628, 1994.

Oguz, T., H. Ducklow, P. Malanotte-Rizzoli, S. Tugrul, N. Nezlin, and U. Unluata, Simulation of annual plankton productivity cycle in the Black Sea by a one-dimensional physical-biological model, *J. Geophys. Res.*, *101*, 16,585–16,599, 1996.

Oguz, T., H. W. Ducklow, P. Malanotte-Rizzoli, J. W. Murray, V. I. Vedernikov, and U. Unluata, A physical-biochemical model of plankton productivity and nitrogen cycling in the Black Sea, *Deep Sea Res., Part I*, *46*, 597–636, 1999.

Oguz, T., H. W. Ducklow, and P. Malanotte-Rizzoli, Modeling distinct vertical biogeochemical structure of the Black Sea: Dynamical coupling of the oxic, suboxic, and anoxic layers, *Global Biogeochem. Cycles.*, *14*, 1331–1352, 2000.

Oguz, T., J. W. Murray, and A. E. Callahan, Modeling redox cycling across the suboxic-anoxic interface zone in the Black Sea, *Deep Sea Res., Part I*, *48*, 761–787, 2001a.

Oguz, T., H. W. Ducklow, J. E. Purcell, and P. Malanotte-Rizzoli, Modeling the response of top-down control exerted by gelatinous carnivores on the Black Sea pelagic food web, *J. Geophys. Res.*, *106*, 4543–4564, 2001b.

Ozsoy, E., U. Unluata, and Z. Top, The evolution of Mediterranean water in the Black Sea: Interior mixing and material transport by double diffusive intrusions, *Prog. Oceanogr.*, *31*, 275–320, 1993.

Samadurov, A. S., and L. I. Ivanov, Process of ventilation of the Black Sea related to water exchange through the Bosphorus, in *Ecosystem Modeling as a Management Tool for the Black Sea*, vol. 2, *NATO ASI Ser. 2: Environmental Security*, vol. 47, edited by L. Ivanov and T. Oguz, pp. 221–235, Kluwer Acad., Norwell, Mass., 1998.

Saydam, C., S. Tugrul, O. Basturk, and T. Oguz, Identification of the oxic/anoxic interface by isopycnal surfaces in the Black Sea, *Deep Sea Res.*, *40*, 1405–1412, 1993.

Tugrul, S., O. Basturk, C. Saydam, and A. Yilmaz, The use of water density values as a label of chemical depth in the Black Sea, *Nature*, *359*, 137–139, 1992.

T. Oguz, Institute of Marine Sciences, Middle East Technical University, P.O. Box 28, Erdemli 33731, Icel, Turkey. (oguz@ims.metu.edu.tr)